

# Image Enhancement ANPSO Processing Technology Based on Improved Particle Swarm Optimization Algorithm

Zhangping You, Dajian Yi, Zheng Fang, Wenhui Zhang

**Abstract**—To improve the efficiency and effectiveness of image enhancement, a novel Ant Colony Natural Inspired Particle Swarm Optimization (ANPSO) algorithm is proposed. This algorithm integrates Ant Colony Optimization (ACO) and Particle Swarm Optimization (PSO) using natural inspiration and chaos theory to enhance image quality. By employing a nonlinear random incremental method, it designs adaptive inertia weights to improve global search capabilities and stability. Furthermore, based on the pheromone release and path optimization mechanisms of the ant colony algorithm, it enhances the information transmission mechanism in PSO, allowing for more efficient information sharing among particles and strengthening cooperative search abilities. Experimental comparisons with Genetic Algorithm (GA), ACO, and PSO demonstrate that ANPSO improves Peak Signal-to-Noise Ratio (PSNR), Structural Similarity Index (SSIM), and algorithm convergence by 8.3%, 7.6%, and 9.7%, respectively. These results highlight the significant performance advantages of ANPSO in image enhancement tasks.

**Index Terms**—Image enhancement; GA; PSO algorithm; ACO algorithm;

## I. Introduction

In recent years, artificial intelligence technology has developed rapidly [1]-[4]. As an intelligent perception technology, computer vision has found extensive applications in various fields such as robotics, fault diagnosis, and remote sensing [5]-[7]. Advances in computer vision technology are reflected not only in algorithm improvements and hardware performance enhancements but also in innovations and expansions in practical applications. In fault diagnosis, computer vision is widely used in equipment monitoring and maintenance, by analyzing image

data to prevent equipment damage and production accidents, significantly enhancing production safety and reliability. In the field of remote sensing, computer vision has become a core tool for analyzing and processing satellite images. Techniques such as contrast enhancement, image segmentation, and feature extraction allow valuable information to be extracted from satellite images, aiding scientists and engineers in monitoring environmental changes, assessing the impact of natural disasters, and planning land use. Additionally, computer vision shows great potential in biomedical image analysis. For example, in medical imaging diagnostics, computer vision technology can assist doctors in more accurately identifying and diagnosing diseases, improving diagnostic efficiency and accuracy.

Contrast enhancement is an image processing technique with two main objectives: first, to increase the difference between objects and background in low dynamic range images, thereby increasing the image's contrast; and second, to reveal image details that may be difficult to perceive otherwise. Images processed with contrast enhancement typically appear more striking subjectively because we can discern differences between objects and background more clearly, making the elements of the image more vivid and distinct. There are several methods of classifying contrast enhancement techniques, including those based on nonlinear functions (such as logarithmic, power-law, and gamma functions), histogram-based techniques, nonlinear filtering, and frequency domain-based methods (such as homomorphic filters). Among these, histogram equalization (HE) is a widely used contrast enhancement technique, commonly applied in fields like radar and medical image processing. However, while histogram equalization (HE) can globally enhance an image, it may lead to over-enhancement issues as it operates based on the most frequently occurring intensity levels in the image. HE also struggles to effectively handle cases where there are significant differences in brightness between the main area of an image and other areas, and it can lead to loss of local details and enhancement of noise. To address these issues, researchers have proposed several improvement methods. Local histogram equalization (LHE), for example, divides the image into small regions and performs histogram equalization on each region, helping to preserve local details and alleviate over-enhancement issues. On the other hand, dualistic sub-image histogram equalization (DSIHE) introduces additional steps of histogram equalization by segmenting and processing the original image, which better handles contrast differences in different regions of the image.

Manuscript received April 29, 2024; revised September 28, 2024.

This work was supported by the National Natural Science Foundation of China (61772247), the Industry-Academia-Research Cooperation Projects of Jiangsu Province (BY2022651), the Key Foundation projects of Lishui(2023LTH03), Discipline Construction Project of Lishui University (Discipline Fund Name: Mechanical Engineering).

Zhangping You is a professor at Lishui University, Lishui 323000, P. R. China (email: 44536388@qq.com).

Dajian Yi is a postgraduate student at Zhejiang Sci-Tech University, Hangzhou 310018, P. R. China (email: ydj1176540684@163.com).

Zheng Fang is an engineer at State Grid Zhejiang Lishui Power Supply Company, Lishui 323000, P. R. China (e-mail: 76896419@qq.com).

Wenhui Zhang is a professor at Nanjing Xiaozhuang University, Nanjing 211171, P. R. China (corresponding author to provide phone: +86-18268906955; e-mail: hit\_zwh@126.com).

Recursive mean separate histogram equalization (RMSHE) uses recursive mean separation to make histogram equalization a progressive process, smoothing the adjustment of the image's contrast. These methods aim to improve upon the shortcomings of HE, such as global over-enhancement and poor adaptability to different brightness regions. Tarik Arici et al. [8] proposed a histogram equalization-based universal framework for image contrast enhancement. By minimizing a cost function in an optimization problem, they introduced a specially designed penalty term to adjust the level of contrast enhancement, achieving a more natural image effect. They also considered factors such as noise robustness, white/black stretching, and average brightness preservation. The proposed low-complexity algorithm demonstrated superior performance. Sara Hashemi et al. [9] proposed an efficient contrast enhancement method based on genetic algorithms. The method uses a simple and novel chromosome representation along with corresponding operators. Experimental results showed that the proposed genetic approach outperforms related methods in contrast and detail enhancement, producing images suitable for consumer electronic products. Sonali et al. [10] proposed a noise removal and contrast enhancement algorithm for fundus images. By combining filtering with Contrast Limited Adaptive Histogram Equalization (CLAHE) technology, they addressed the denoising and enhancement issues of color fundus images. Wang et al. [11] proposed a color image correction method based on non-linear function transformation to improve the adaptability of image enhancement to low-light images. Based on the illumination-reflection model and multi-scale theory, the algorithm can enhance the overall brightness and contrast of images while reducing the impact of uneven illumination.

Automatic contrast enhancement techniques are highly demanded in many application scenarios. However, automating these algorithms is challenging because it requires evaluating objective functions that measure the quality of the enhanced images. To address this issue, a series of optimization methods based on neural network evolutionary computation have been proposed in recent years, aiming to achieve automatic execution of contrast enhancement tasks [12]-[14]. The key goal of these techniques is to find the optimal parameter settings or the best input/output mapping to produce the highest quality images.

In recent years, many studies have proposed contrast enhancement methods based on optimization algorithms. C. Narmatha et al. [15] proposed a fuzzy brainstorming optimization algorithm for medical image segmentation and classification, which combines fuzzy and brainstorming optimization techniques. The brainstorming optimization focuses on the cluster center and gives it the highest priority, while the fuzzy part iterates multiple times to present the best network structure. Zhuang et al. [16] developed a Bayesian retinal algorithm to enhance a single underwater image using multi-stage gradients of reflectance and illumination as priors, transforming the complex problem of underwater image enhancement into two simpler denoising problems. They provided their convergence analysis mathematically and derived their solutions through efficient optimization

algorithms. F. Orujov et al. [17] developed an image processing algorithm based on contour detection, which uses Mamdani (Type-2) fuzzy rules, contrast-limited adaptive histogram equalization (CLAHE) for contrast enhancement, and median filtering for background exclusion. This method, as a flexible approach, is applicable to a variety of edge detection/contour-based applications.

Although researchers have made significant efforts to improve the performance of image contrast enhancement, research on contrast enhancement for industrial images remains relatively limited. Therefore, we propose an innovative industrial image contrast enhancement technique based on an improved PSO algorithm (named ANPSO) and apply it to local/global image enhancement. The innovations of this paper can be summarized as follows:

(1) Designing a chaotic mapping based on the performance of particles and the distance from their optimal positions to construct nonlinear random increment inertia weights, achieving a random chaotic distribution of each particle in different dimensions, and improving the global search effectiveness of the algorithm.

(2) By introducing adaptive inertia weights into the PSO algorithm, the stability of the algorithm is improved. At the same time, by using the information transmission mechanism of the ant colony algorithm, the ant colony algorithm is integrated with the improved PSO to design a new APSO algorithm, which achieves information sharing between particles, and improves the effectiveness of cooperation and collaborative search.

(3) Based on the mechanism of releasing pheromones in the ant colony algorithm to attract other particles to form the optimal path, a heuristic-based data selection and updating algorithm is designed to enhance the optimization strength of the algorithm, improve spatial search capabilities, and accelerate convergence speed.

The rest of the paper is organized as follows: Section 2 introduces the principles of LGE enhancement transformation and the original PSO algorithm. Section 3 details the proposed ANPSO algorithm. Section 4 presents the experimental results and discusses them. Section 5 draws conclusions and suggests future work.

## II. Image Enhancement Transformations

### A. Local/Global Enhancement Transformations

Local/Global Enhancement (LGE) transformation utilizes both local statistical information of the image (e.g., mean, variance) and global image information. This function is an extended version of the local enhancement function. For each pixel located at position  $(u, v)$  in an image of size  $M \times N$ , the transformation  $T_{LGE}$  is applied to map the old intensity  $f(u, v)$  to a new intensity value  $g(u, v)$ . The expression for the LGE transformation is:

$$g(u, v) = T_{LGE}[f(u, v)] = k * \frac{G_m}{\sigma(u, v) + b} [f(u, v) - c * m(m, v)] + (u, v)^a \quad (1)$$

Where  $u = 0, 1, \dots, M-1, v = 0, 1, \dots, N-1$  is the global average value of the original image, and  $G_m$  is the new intensity value.

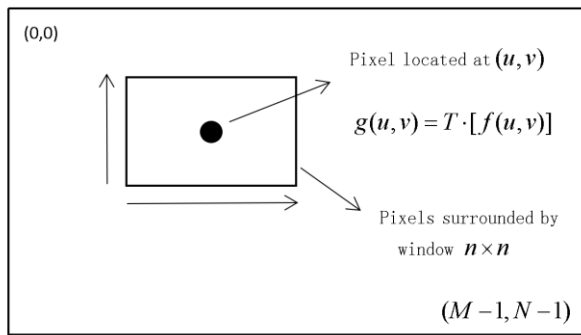


Fig. 1 Local Image Statistics with an  $n \times n$  Window

As shown in Fig.1, the local statistics for a window size of  $n \times n$ , including the mean  $m(u, v)$  and the standard deviation  $\sigma(u, v)$ , are calculated as follows:

$$m(u, v) = \frac{1}{n^2} \sum_{i=-\text{int}n/2}^{\text{int}n/2} \sum_{j=-\text{int}n/2}^{\text{int}n/2} f(u+i, v+j) \quad (2)$$

$$\sigma(u, v) = \sqrt{\frac{1}{n^2} \sum_{i=-\text{int}n/2}^{\text{int}n/2} \sum_{j=-\text{int}n/2}^{\text{int}n/2} (f(u+i, v+j) - m(u+i, v+j))^2} \quad (3)$$

The global mean of image  $G_m$  is calculated as:

$$G_m = \frac{1}{M \times N} \sum_{u=0}^{M-1} \sum_{v=0}^{N-1} f(u, v) \quad (4)$$

From formula (2), it can be seen that the four unknown parameters a, b, c, and k have a significant impact on the LGE transformation. Parameter a introduces smoothing and brightness effects in the image, parameter b introduces an offset to the standard deviation in the neighborhood. Parameter c is used to control how much of the average value is subtracted from the image  $f(u, v)$ . Finally, parameter k controls the global enhancement of the image.

### B. Objective Function

In the absence of external intervention, automatically measuring the quality of enhanced images requires defining a suitable objective function. Various objective functions have been proposed in the literature, and the objective function (fitness value) used in this paper can quantify the quality of image enhancement, making it suitable for automated performance evaluation. It is shown below:

$$F(I_e) = \ln[\ln(E(I_e)) + \exp] * \frac{\text{edgels}(I_e)}{M \times N} \exp(H(I_e)) \quad (5)$$

Where  $I_e$  is the enhanced image generated after processing by the transformation function,  $\text{edgels}(I_e)$  represents the number of edge pixels obtained from  $I_e$  by the Sobel edge detector,  $E(I_e)$  is the sum of edge strengths of the enhanced image, and  $H(I_e)$  represents the entropy value of  $I_e$ .

The formula to calculate  $H(I_e)$  is as follows:

$$H(I_e) = \begin{cases} -\sum_i V_i \log_2(V_i), & V_i \neq 0 \\ 0, & V_i = 0 \end{cases} \quad (6)$$

Where  $i \in \{1, 2, \dots, 256\}$  is an 8-bit grayscale image and  $V_i$  is the probability of occurrence of the  $i$ -th gray level.

The formula to calculate  $E(I_e)$  is as follows:

$$E(I_e) = \sum_u \sum_v \sqrt{S_{h1}(u, v)^2 + S_{v1}(u, v)^2} \quad (7)$$

The formula denotes that  $S_{h1}(u, v)$  and  $S_{v1}(u, v)$  are horizontal and vertical Sobel template edge detections, respectively.

The Sobel operator is a typical image enhancement operator used primarily for edge detection. It is based on the gradient information of the image and can effectively extract edge features from the image. The Sobel operator uses two  $3 \times 3$  convolution kernels, one for detecting horizontal edges and the other for detecting vertical edges. By applying these two convolution kernels to the pixels of the image, the gradient magnitude and direction of each pixel can be calculated.

Histogram equalization is a method to transform the original image into a new image with a histogram that is uniformly distributed. Let r and s represent the normalized grayscale values of the original image and the image after histogram equalization, respectively. That is,  $0 \leq r, s \leq 1$ . For any r value in the  $[0, 1]$  interval, there is a corresponding s value, and  $s = T(r)$ . The inverse transformation relationship is  $r = T^{-1}(s)$ . According to probability theory, if the probability density function of the random variable r is  $p_r(r)$ , and the random variable s is a function of r, then the probability density  $p_s(s)$  of s can be derived from  $p_r(r)$ . Assuming the distribution function of the random variable s is represented by  $F_s(s)$ , according to the definition of distribution function:

$$F_s(s) = \int_{-\infty}^s p_s(s) ds = \int_{-\infty}^r p_r(r) dr \quad (8)$$

By using the relationship that the density function is the derivative of the distribution function, we can differentiate both sides of the equation with respect to s:

$$p_s(s) = \frac{d}{ds} \left[ \int_{-\infty}^r p_r(r) dr \right] = p_r \frac{dr}{ds} = p_r \frac{d}{ds} [T^{-1}(s)] \quad (9)$$

As can be seen, the probability density function of the output image can be adjusted to a uniformly distributed histogram by the transformation function  $T(r)$ . This corrected image can meet the requirements of human visual perception. Fig. 2 shows the original image, the image enhanced by the Sobel operator, and the image enhanced by histogram equalization.

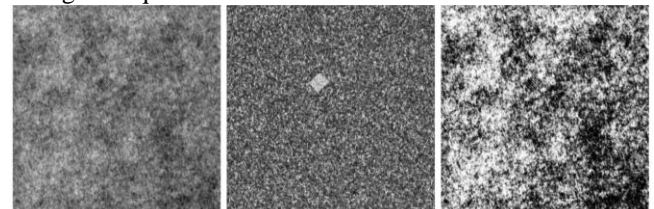


Fig. 2 The original image, the image enhanced by Sobel operator, and the image enhanced by histogram equalization.

### C. Particle Swarm Optimization Algorithm

The Particle Swarm Optimization (PSO) algorithm is a widely acclaimed optimization tool used for optimizing features by performing iterative local and global searches in feature space to find significant features. The algorithm's

population consists of a group of random particles that continuously move in feature space, seeking the optimal solution through continuous iterations. This process continues until an appropriate convergence level is reached. PSO simulates the collaborative behavior of a particle swarm, enabling each particle to adjust its search position based on individual experience and information from the entire swarm, thereby efficiently finding the global optimal solution in the search space.

The basic Particle Swarm Optimization (PSO) algorithm updates particles based on their individual historical best position ( $p_{best}$ ) and the global best position of the swarm ( $g_{best}$ ) to find the optimal particle. For solving an optimization problem with variables  $X = \{X_1, X_2, \dots, X_D\}$  and objective function  $\min\{f(x)\}$ , the basic PSO algorithm's particle update formula is given by [18]:

$$v_{id}(t+1) = wv_{id}(t) + c_1r_1(p_{best_{id}} - x_{id}(t)) + c_2r_2(g_{best_g} - x_{id}(t)) \quad (10)$$

$$x_{id}(t+1) = x_{id}(t) + v_{id}(t+1) \quad (11)$$

The formula consists of the following variables:  $v_{id}(t+1)$  and  $x_{id}(t+1)$  represent the velocity and position of particle  $i$  at iteration  $t+1$ ;  $w$  is the inertia weight, which decreases with the number of iterations in the standard PSO algorithm;  $c_1$  and  $c_2$  are the cognitive and social learning factors, typically set to 2;  $r_1$  and  $r_2$  are random numbers uniformly distributed between 0 and 1.

In the equation above,  $r_1$  and  $r_2$  are two increasing random numbers, ranging from 0 to 1, while  $c_1$  and  $c_2$  represent the weighting parameters of individual and social influences. The update velocity equation consists of three independent parts: the inertia component, the individual cognitive component, and the social contact component. In the search algorithm, the weight parameter  $w$  plays a balancing role in the inertia component. In the second part (individual cognition), information updates are based on the particle's local knowledge. Finally, in the third part, updates are made based on cooperation among particles. Fig. 3 shows the variation of inertia weight with iteration times in standard particle swarm optimization.

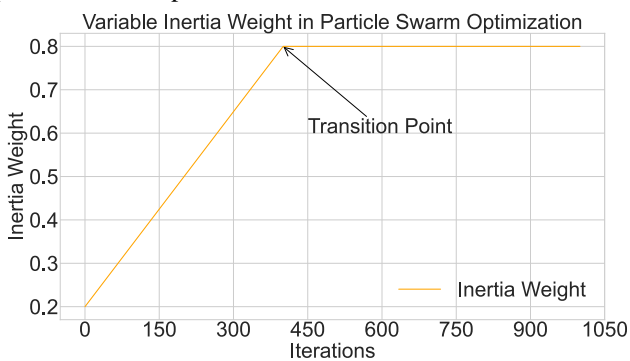


Fig. 3 Changes in Inertia Weight with Iteration Count in Standard Particle Swarm Optimization

### III. The proposed ANPSO algorithm

#### A. Introducing Chaotic Mapping for Nonlinear Random Increment of Inertia Weight

The inertia weight is an important parameter in the Particle Swarm Optimization (PSO) algorithm, playing a crucial role in balancing the algorithm's global exploration and local exploitation capabilities. Traditional PSO algorithms use linearly decreasing inertia weights to balance the algorithm's exploitation and exploration capabilities to some extent. However, when dealing with complex nonlinear multidimensional function optimization problems, the algorithm is prone to getting stuck in local optima. Feng et al. [19] introduced two improved methods for PSO, both using chaos theory to adjust the inertia weight. The first method is chaotic decreasing inertia weight, and the second method is chaotic random inertia weight. In this study, the latter is considered the inertia weight parameter that enhances PSO performance. The use of dynamic chaotic random inertia weight aims to achieve a balance between exploitation and exploration. A low inertia weight helps strengthen the exploitation process, while a high inertia weight is beneficial for exploring a wider search space. Compared to static inertia weights, dynamic chaotic random inertia weights can maintain the algorithm's diversity, avoid premature convergence to local optima, and improve the global search performance of PSO. The reason for choosing this approach of chaotic search optimization is because chaos has highly dynamic characteristics, which helps maintain the diversity of the particle swarm and avoids local optima while searching for the global optimum.

The logic mapping  $Z_{t+1} = \mu Z_t(1 - Z_t)$ , where  $\mu = 4$  is a very common chaotic map, cannot guarantee that the initial values of  $Z_0 \notin \{0, 0.25, 0.5, 0.75, 1\}$  generated in the initial generation process are chaotic. In this paper, the sine chaotic map given by formula (11) is used to avoid this drawback.

$$Z_{t+1} = \beta \sin(\pi \cdot Z_t) \quad (12)$$

Where  $\beta > 0$ ,  $Z_t, Z_{t+1} \in [0, 1]$ , and  $t$  are generated numbers, in some instances, the value of  $Z_{t+1}$  is relatively small. Therefore, to improve the effectiveness of chaotic random inertia weights in particle swarm optimization, the original chaotic formula is modified as follows:

$$Z_{t+1} = \left| \sin\left(\frac{\pi Z_t}{rand(\cdot)}\right) \right| \quad (13)$$

Where  $\beta = 1$  and  $Z_t, Z_{t+1} \in [0, 1]$ ; the absolute value ensures that the next generation process of chaotic space has  $Z_{t+1} \in [0, 1]$ . Therefore, the chaotic inertia weight is given by the following equation:

$$w_c^f = 0.5 \times rand(\cdot) + 0.5 \times z_{t+1} \quad (14)$$

To prevent particles from diverging when searching for solutions in the problem space, an  $\lambda$  coefficient is used to fine-tune the convergence of particle swarm optimization:

$$\lambda = \frac{2}{(\phi - 2 + \sqrt{\phi^2 - 4\phi})} \quad (15)$$

Parameter  $\phi = m_1 + m_2$  depends on cognitive and social parameters, while  $\phi > 4$  ensures the effectiveness of the contraction coefficient. Introducing both cognitive and social parameters into PSO, by making the cognitive component larger and the social component smaller during initialization or early evolution stages, enhances both local

and global search. As evolution progresses, the linearly decreasing cognitive component and linearly increasing social component strengthen the exploitation and exploration capabilities of the particle swarm algorithm, helping it to converge to the global optimum more effectively.

$$m_1^t = m_{1,f} - \frac{t}{P}(m_{1,f} - m_{1,i}) \tag{16}$$

$$m_2^t = m_{2,f} - \frac{t}{P}(m_{2,f} - m_{2,i}) \tag{17}$$

Where  $m_{1,i}$ ,  $m_{2,i}$ ,  $m_{1,f}$ , and  $m_{2,f}$  are the initial and final values of the cognitive and social parameters;  $t$  is the current generated value, and  $P$  is the final generated value. Combining the above coefficients ensures the convergence quality of particle swarm optimization and the stability of the generation process.

**B. Ant Colony Optimization Algorithm**

ACO (ant colony optimization) [20] is a heuristic algorithm introduced by Marco Dorigo in 1997, demonstrating the potential to solve the Traveling Salesman Problem (TSP). The algorithm simulates the natural behavior of ants in finding food through pheromone trails. In this method, agents (simulated ants) communicate through pheromones to simulate the communication between ants, transmitting information about finding the shortest path. The goal of TSP is to find the best global travel route, covering all cities and returning to the starting point. Ants accumulate information during the search process to generate short trips. They use pheromone trails on the path to select the next city to visit, preferring cities with more pheromones. In the initial stage, ants randomly select a city, and then through the iterative process, they continuously update their pheromones until the travel task is completed. Finally, using the pheromone trail update equation (11), ants with the shortest paths will update the global path GT. equation (10) is used to evaluate the path selection probability from node  $i$  to node  $j$ . Where  $\Omega_i$  represents the concentration of pheromones between nodes  $i$  and  $j$ ,  $\tau_{i,j}$  represents the domain of the  $i$ -th node, and  $a$  and  $b$  are the adjustment parameters of the pheromones.  $P$  represents the probability that ant( $k$ ) chooses to pass through the arc ( $i, j$ ).

$$P_{i,j}^k = (\tau_{i,j}^{k-1})^a * \eta_{i,j}^\beta + \sum_{j \in \Omega_i} (\tau_{i,j}^{k-1})^a * \eta_{i,j}^\beta \tag{18}$$

The ants need to choose  $P_{i,o}^k$ ,  $P_{i,j}^k$ ,  $P_{i,l}^k$ , and  $P_{i,m}^k$  in their food search process to pass from the current city  $i$  to another city ( $j, l, m, o$ ), as shown in Fig. 4. They start locally, assume a city, move from one node to another, and eventually return to the starting point, using the shortest path. Pheromones act as markers for paths in the search space, reflecting the paths most frequently used globally, helping to avoid getting stuck in local optima. To update the pheromones, formula (11) is used, where  $\rho$  is the pheromone evaporation coefficient.

$$\text{if } (i, j) \in \text{BestTour} \tau_{ij} = (1 - \rho)\tau_{ij}^{(k-1)} + \rho\Delta_{ij}^k$$

$$\text{else } \tau_{ij}^{(k-1)} = \tau_{ij}^{(k-1)} \tag{19}$$

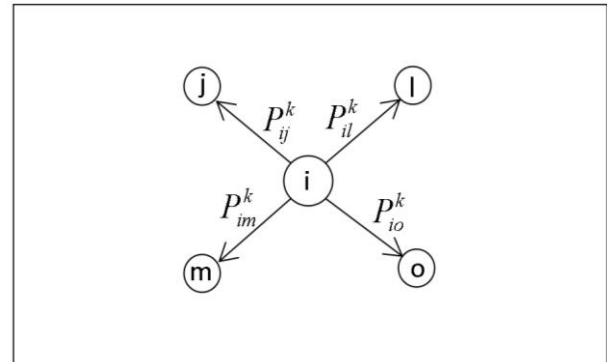


Fig. 4 Random Ant Policy

**C. Implementation of the Algorithm**

The principle of the ANPSO algorithm is to create a hybrid improvement algorithm based on the Particle Swarm Optimization (PSO) algorithm, specifically tailored for image enhancement applications. This algorithm introduces a chaotic Sine mapping to construct a nonlinear random incremental inertia weight, which makes the initial positions and velocities of particles more random. The ANPSO algorithm also combines elements from the Ant Colony Optimization (ACO) algorithm. It considers the principle of pheromones left by ants when updating their positions and velocities, which enhances the efficiency and accuracy of particle position updates. Moreover, when reselecting particles based on the pheromones left by previous particles and the paths constructed, the final aggregated new particle swarm will be superior, leading to better optimized results. The iterative transformation diagram of the inertia weight nonlinear random incremental adaptive chaotic mapping is shown in Fig. 5.

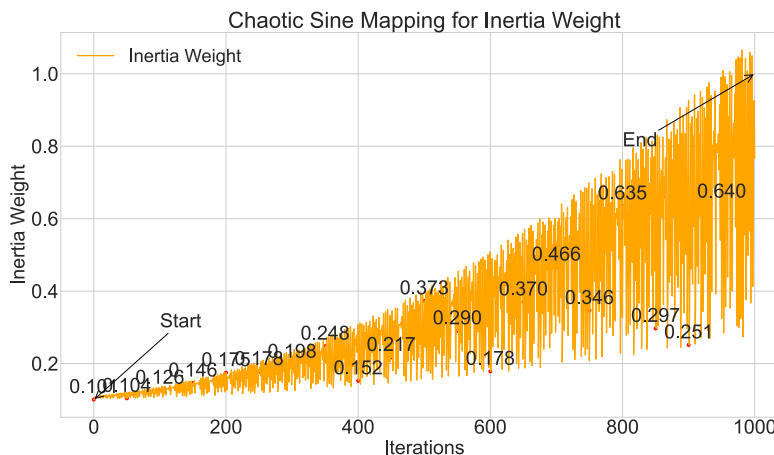


Fig. 5 Iteration Transformation of Adaptive Chaotic Mapping for Nonlinear Random Increment of Inertia Weight

Table I Pseudocode of the ANPSO

|   |
|---|
| The proposed ANPSO algorithm  |
| Initialize the particle swarm and ant colony  |
| Initialize the chaotic inertia weight   |
| Evaluate the current particle mass  |
| <b>while</b> the individual particle mass has not reached the optimal quality <b>do</b>                 |
| Particles randomly disperse, select a group, and leave behind pheromones                                |
| Particles create optimal paths based on pheromones and select a new group                               |
| <b>if</b> ( $i > p_{best}$ ) <b>do</b>  |
| Update the chaotic inertia weight   |
| Chaotic particle random distribution  |
| Update individual best quality and position   |
| <b>end</b>  |
| <b>if</b> ( $i > g_{best}$ ) <b>do</b>  |
| Update global best quality and particle   |
| Update the best particle mass   |
| <b>end</b>  |
| Update the velocity and position of the best chaotic particle   |
| Define a function for updating particle positions   |
| Calculate the new velocity using inertia weight, individual learning factor, and social learning factor |
| Calculate the new position using the new velocity   |
| Update the best particle swarm  |
| <b>end</b>  |
| <b>Return</b> the optimal solution and the objective function   |

#### IV. Experiment and Result Analysis

In this chapter, we evaluated the performance of the proposed ANPSO algorithm in a series of industrial image enhancement experiments. Firstly, we used the image enhancement evaluation metrics PSNR and SSIM to evaluate the optimization ability of the ANPSO algorithm in image enhancement experiments. Then, we conducted visual comparison experiments to intuitively feel the image enhancement effect of the ANPSO algorithm. Finally, we compared the convergence of the ANPSO algorithm with several other image enhancement optimization algorithms to comprehensively demonstrate the superiority of the proposed ANPSO algorithm. Table I shows the ANPSO pseudocode, while Fig. 6 shows the ANPSO flowchart.

In this section, some typical optimization algorithms such as GA, ACO, original PSO, HE, and SA are used to compare with the proposed ANPSO algorithm in this paper. Tables II to VI show the various parameter settings for each algorithm.

Table II Parameter setting for GA algorithm

| Parameter             | Setting |
|-----------------------|---------|
| Population Size       | 100     |
| Crossover Probability | 0.8     |
| Mutation Probability  | 0.05    |
| Number of Generations | 50      |

Table III Parameter setting for ACO algorithm

| Parameter                  | Setting |
|----------------------------|---------|
| Number of Ants             | 100     |
| Pheromone Evaporation Rate | 0.25    |
| Pheromone Intensity        | 5       |
| Heuristic Factor           | 3       |
| Exploration Probability    | 0.25    |

Table IV Parameter setting for PSO algorithm

| Parameter                  | Setting |
|----------------------------|---------|
| Number of Particles        | 80      |
| Inertia Weight             | 0.5     |
| Individual Learning Factor | 1       |
| Social Learning Factor     | 1       |
| Max Velocity Limit         | 5%      |

Table V Parameter setting for SA algorithm

| Parameter                  | Setting |
|----------------------------|---------|
| Initial Temperature        | 1000    |
| Final Temperature          | 0.01    |
| Cooling Rate               | 0.95    |
| Iterations per Temperature | 100     |

Table VI Parameter setting for HE algorithm

| Parameter             | Setting |
|-----------------------|---------|
| Number of Gray Levels | 256     |

##### A. Evaluation Metrics

PSNR (Peak Signal-to-Noise Ratio) and SSIM (Structural Similarity Index) are common metrics used to evaluate image quality, particularly suitable for performance evaluation of image enhancement algorithms [21]. PSNR is a metric used to measure the degree of quality loss in an image. It calculates the mean square error between the original image and the processed image and converts it into a more readable unit in decibels. A higher PSNR value indicates that the processed image is more similar to the original image. The formula for calculating PSNR is:

$$PSNR = 20 * \log_{10} \left( \frac{Q-1}{RMSE} \right) \quad (20)$$

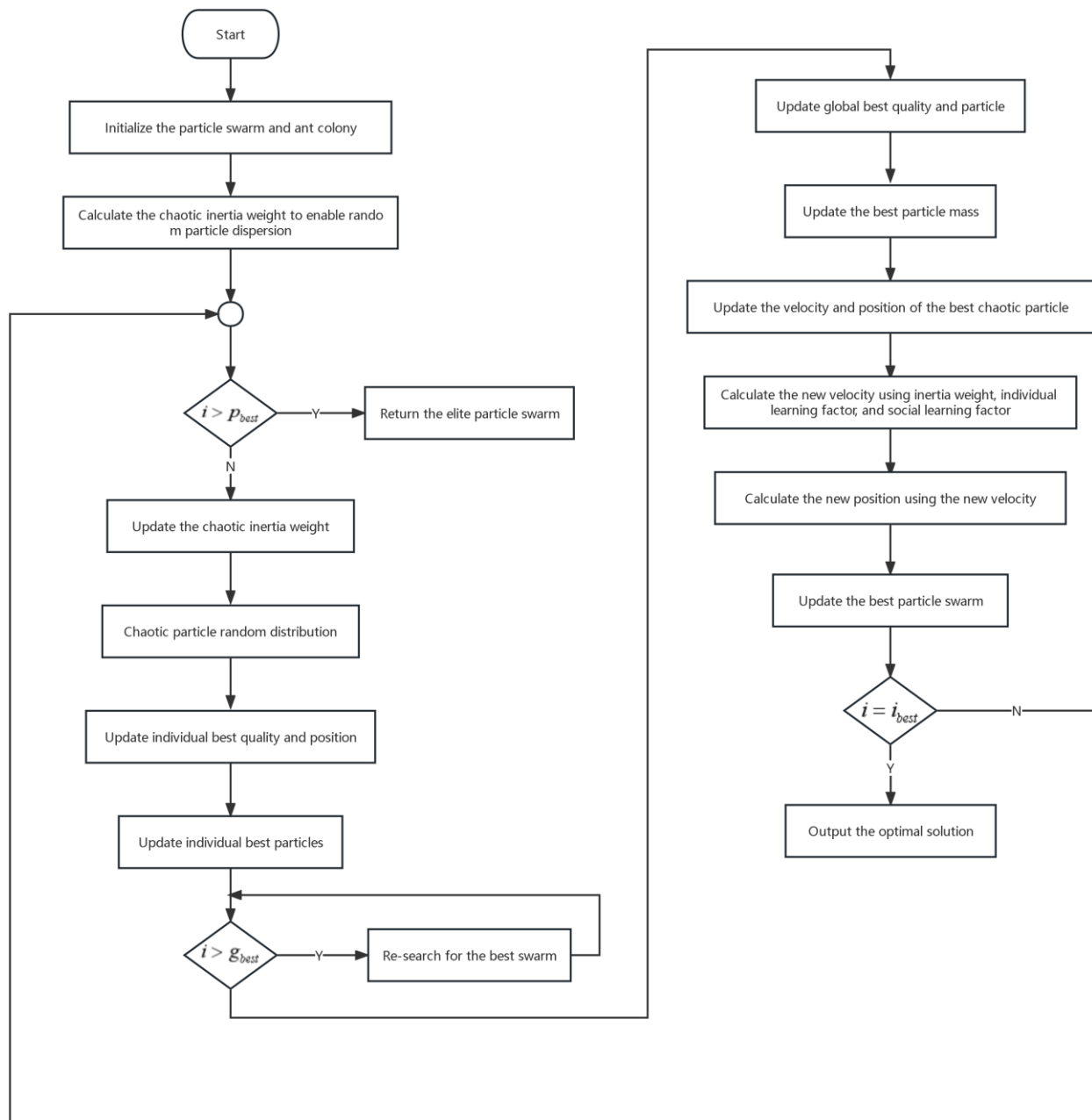


Fig. 6 Flowchart of the ANPSO

Where  $L$  represents the possible intensity levels in the image, and RMSE is the root mean square error, which can be determined by the following equation:

$$RMSE = \left( \frac{1}{MN} \sum_{x=0}^{M-1} \sum_{y=0}^{N-1} |I_i - D_o|^2 \right)^{\frac{1}{2}} \quad (21)$$

Where  $D_o$  represents the data of the degraded image,  $I_i$  represents the input data of the original image,  $M$  and  $N$  represent the number of pixels in rows and columns, and  $x$  and  $y$  represent the indices of the corresponding column and row in the image. The experimental results show that the PSNR (peak signal-to-noise ratio) value does not completely reflect the actual perception of the image by the human eye. Although PSNR is often used to measure the quality of image reconstruction, human visual sensitivity to different errors is complex, and PSNR fails to fully consider these perceptual factors. Therefore, in evaluating image quality, in

addition to PSNR, other visual quality evaluation metrics should be combined to more accurately reflect the human eye's perception of image details and structure.

The structural similarity index (SSIM) is a more complex metric that considers not only the similarity of pixel values but also factors such as brightness, contrast, and structure. The calculation formula for SSIM includes three components: luminance similarity, contrast similarity, and structure similarity. The overall SSIM value is obtained by the weighted average of these three components. Fig. 7 shows the SSIM values of GA, ACO, PSO, and ANPSO optimization algorithms for three types of random image enhancement.

$$SSIM(x, y) = \frac{(2\mu_x \mu_y + d_1)(2\sigma_{xy} + d_2)}{(\mu_x^2 + \mu_y^2 + d_1)(\sigma_x^2 + \sigma_y^2 + d_2)} \quad (21)$$

Where  $x$  and  $y$  are the reference and segmented



images,  $\mu_x$  and  $\mu_y$  are the mean values of  $x$  and  $y$  respectively,  $\sigma_x$  and  $\sigma_y$  are the mean standard deviations of  $x$  and  $y$  respectively, and  $\sigma_{xy}$  represents the covariance of  $x$ ,  $d_1 = (K_1 L)^2$ ,  $d_2 = (K_2 L)^2$ , Where  $K_1 \ll 1$  and  $K_2 \ll 1$ . From the Table VII, it can be seen that

in the six different image enhancement experiments, compared to the common genetic algorithm, original ant colony algorithm, HE algorithm, BA algorithm, and original PSO algorithm, the ANPSO optimization algorithm used in this paper has a more stable and higher PSNR value in image enhancement experiments, with an average improvement of about 8.3%, showing significant advantages.

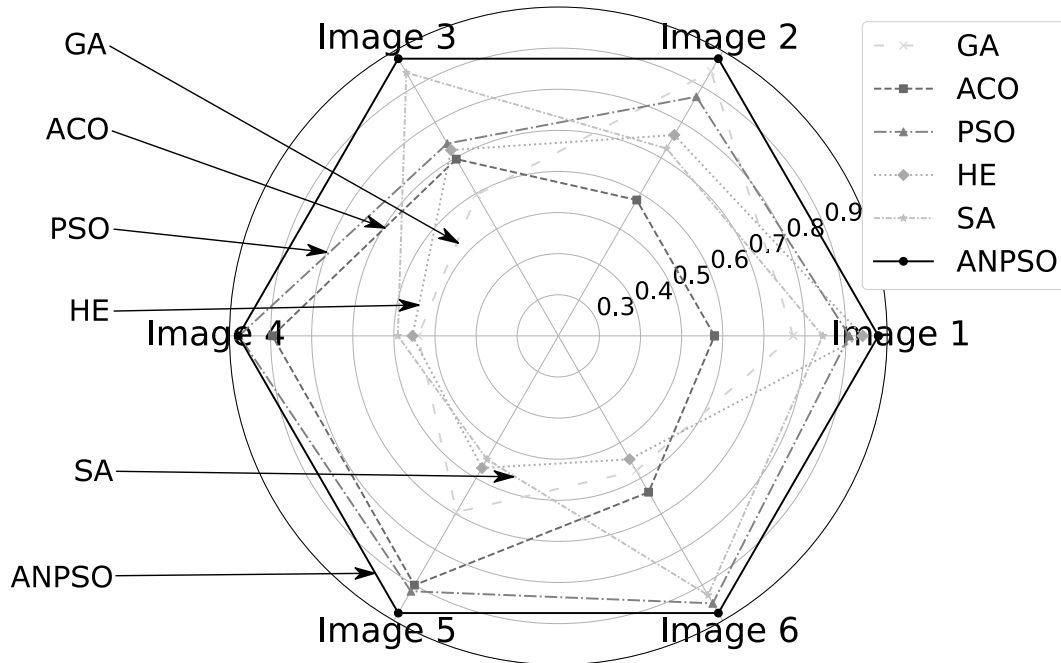


Fig.7 SSIM Values of GA, ACO, PSO and ANPSO Optimization Algorithm in Three Random Image Enhancements

Table VII PSNR Data for Six Image Enhancement Algorithms in Six Different Image Enhancement Experiments

| Image        | Index  | Result  |         |         |          |         |         |
|--------------|--------|---------|---------|---------|----------|---------|---------|
|              |        | GA      | ACO     | PSO     | HE       | BA      | ANPSO   |
| Test image 1 |        |         |         |         |          |         |         |
|              | Best   | 39.0143 | 37.3235 | 39.3982 | 30.4951  | 32.2371 | 39.7564 |
|              | Worst  | 23.1204 | 21.1617 | 20.4117 | 23.6681  | 22.7899 | 24.2153 |
|              | Median | 31.9732 | 32.0223 | 24.2468 | 26.0848  | 27.3272 | 33.1165 |
|              | Mean   | 31.2477 | 29.5578 | 28.8684 | 26.9423  | 27.4637 | 31.9859 |
|              | Std    | 6.1749  | 7.0625  | 8.5390  | 2.6554   | 3.5363  | 2.4722  |
| Test image 2 |        |         |         |         |          |         |         |
|              | Best   | 33.1521 | 30.8382 | 34.1173 | 37.9384  | 30.9446 | 38.0624 |
|              | Worst  | 21.4919 | 20.1665 | 24.9531 | 21.6404  | 20.7585 | 25.7712 |
|              | Median | 27.7315 | 25.7139 | 27.4419 | 31.1586  | 29.6512 | 33.9531 |
|              | Mean   | 27.0626 | 26.0152 | 28.3274 | 30.4521  | 26.637  | 36.0077 |
|              | Std    | 4.8955  | 3.9249  | 3.572   | 5.8602   | 5.2355  | 2.1852  |
| Test image 3 |        |         |         |         |          |         |         |
|              | Best   | 37.2182 | 38.2643 | 35.1346 | 35.4026  | 37.4379 | 40.9542 |
|              | Worst  | 28.9309 | 29.5876 | 23.5361 | 20.3666  | 28.207  | 32.6421 |
|              | Median | 34.4577 | 33.6638 | 33.9691 | 33.5628  | 32.7557 | 36.7745 |
|              | Mean   | 33.4184 | 33.3419 | 31.5983 | 30.6925  | 32.3336 | 38.8643 |
|              | Std    | 3.8421  | 3.2821  | 4.7697  | 6.0432   | 4.0902  | 3.0261  |
| Test image 4 |        |         |         |         |          |         |         |
|              | Best   | 39.9822 | 39.8152 | 38.7665 | 29.5315  | 38.8393 | 43.4629 |
|              | Worst  | 21.1803 | 24.5892 | 22.1471 | 22.1039  | 23.6545 | 36.4921 |
|              | Median | 23.5429 | 32.2793 | 35.9313 | 24.2097  | 38.2655 | 40.1233 |
|              | Mean   | 29.3495 | 32.4681 | 32.6332 | 25.0523  | 34.7756 | 41.0642 |
|              | Std    | 9.4273  | 7.0620  | 7.4349  | 3.2627   | 6.4833  | 3.0116  |
| Test image 5 |        |         |         |         |          |         |         |
|              | Best   | 39.6937 | 38.7112 | 38.4856 | 35.8182  | 31.0891 | 41.3478 |
|              | Worst  | 29.9532 | 28.9623 | 20.3694 | 24.5228  | 22.6054 | 36.6289 |
|              | Median | 38.1521 | 31.7718 | 22.8922 | 33.3083  | 27.0909 | 38.6324 |
|              | Mean   | 35.4624 | 33.4323 | 26.1206 | 31.9255  | 26.9126 | 39.7632 |
|              | Std    | 4.6034  | 4.5218  | 7.4172  | 4.4331   | 4.1922  | 3.1152  |
| Test image 6 |        |         |         |         |          |         |         |
|              | Best   | 38.9296 | 35.3993 | 34.7563 | 36.876   | 38.4009 | 40.5625 |
|              | Worst  | 23.1361 | 23.6451 | 24.4853 | 20.0169  | 22.4525 | 26.6722 |
|              | Median | 36.3152 | 29.8985 | 30.8749 | 26.2506  | 35.8746 | 37.7371 |
|              | Mean   | 33.9715 | 29.8516 | 29.5394 | 27.48216 | 33.0721 | 35.2877 |
|              | Std    | 6.2835  | 4.8884  | 4.1243  | 6.5393   | 6.4695  | 3.6482  |



From Fig. 8, it can be seen that in three random image enhancement experiments, the genetic algorithm and the original PSO algorithm both exhibit significant instability in SSIM values. This indicates that these image enhancement methods are prone to distorting images and introducing more noise. Although the original ant colony algorithm shows relatively stable SSIM values in image enhancement experiments, its average SSIM value is lower compared to the ANPSO optimization algorithm proposed in this paper. The ANPSO optimization algorithm proposed in this paper has an average improvement of about 7.6% in the SSIM enhancement effect experiment compared to the other three algorithms.

*B. Visualized Image Enhancement Experiments*

The ANPSO algorithm used in this paper for image enhancement is verified by selecting one image each of six types of defective images from a network database for method effectiveness validation. The original images and their grayscale histograms are shown in the figure below. To demonstrate the superiority of the image enhancement method based on the ANPSO algorithm used in this paper, comparisons are made with genetic algorithm, original ant colony algorithm, and original PSO algorithm.

The following Fig. 9 shows the visual comparison of the enhancement effects of surface defects in four types of

products using genetic algorithm, original ant colony algorithm, original PSO algorithm, and the ANPSO optimization algorithm used in this paper for image enhancement. The genetic algorithm, while capable of enhancing contrast and preserving details in local regions, tends to introduce problems such as over-enhancement, noise amplification, complex texture distortion, and motion artifacts. In the image enhancement experiments of oil stains, surface damage, and surface scratches on steel surfaces, the genetic algorithm exhibited a significant problem of disappearing detailed defect characteristics. The ant colony algorithm can adjust brightness and contrast, but it may lead to information loss, color distortion, nonlinear transformations, and changes in image appearance, similar to the issues seen with the genetic algorithm. The ant colony algorithm can effectively enhance the contrast of images, but it may also lead to problems such as global equalization, noise enhancement, loss of local details, over-enhancement, and distortion. In the image enhancement experiments of oil stains on steel surfaces and scratches on wood surfaces, the ant colony algorithm exhibited problems of excessive enhancement of the background and merging of defect features. Through comparison, it is found that the product surface defect image enhancement effect using the ANPSO optimization algorithm proposed in this paper is better.

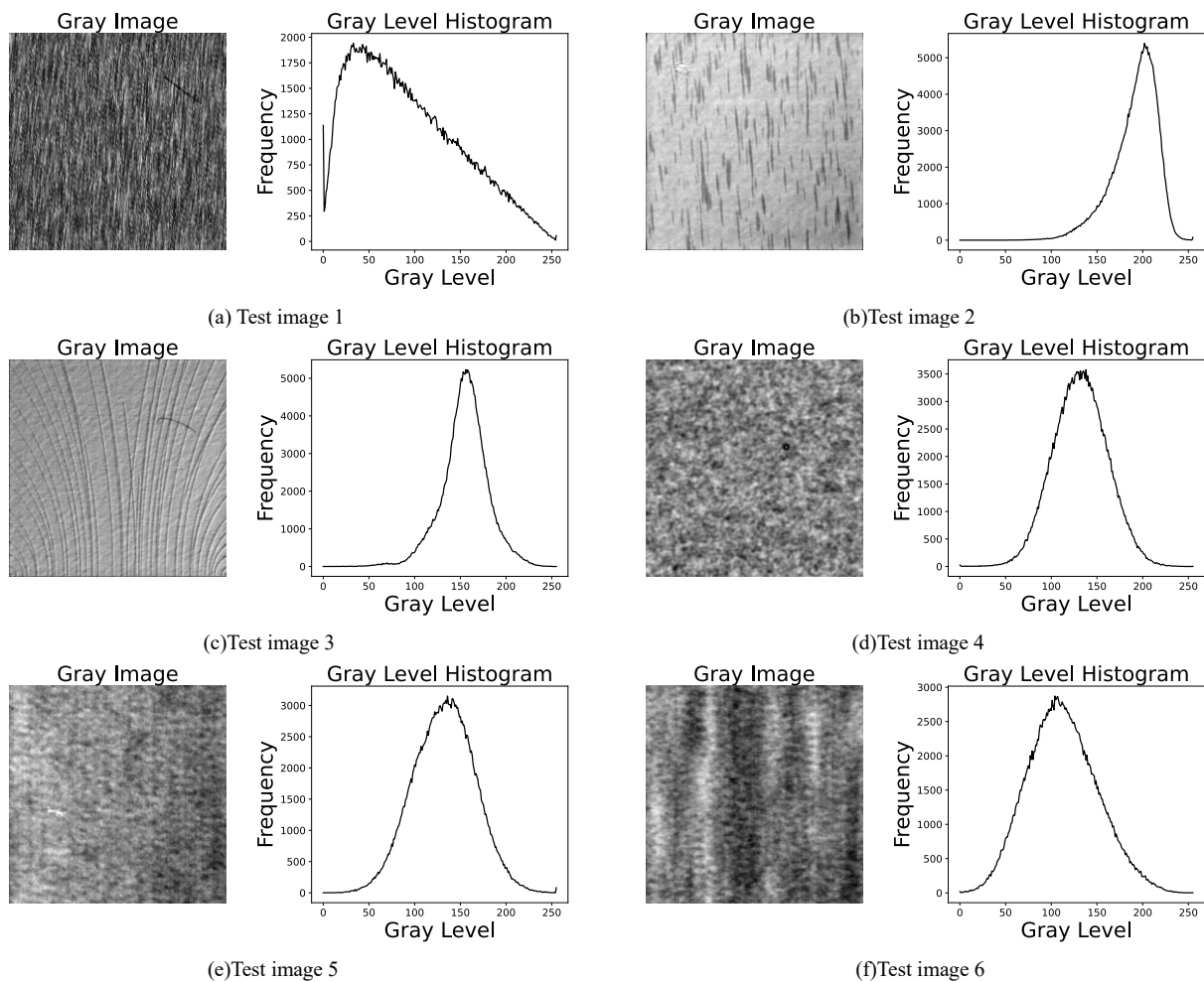


Fig. 8 Original Images and Their Grayscale Histograms of Common Defects in Various Products

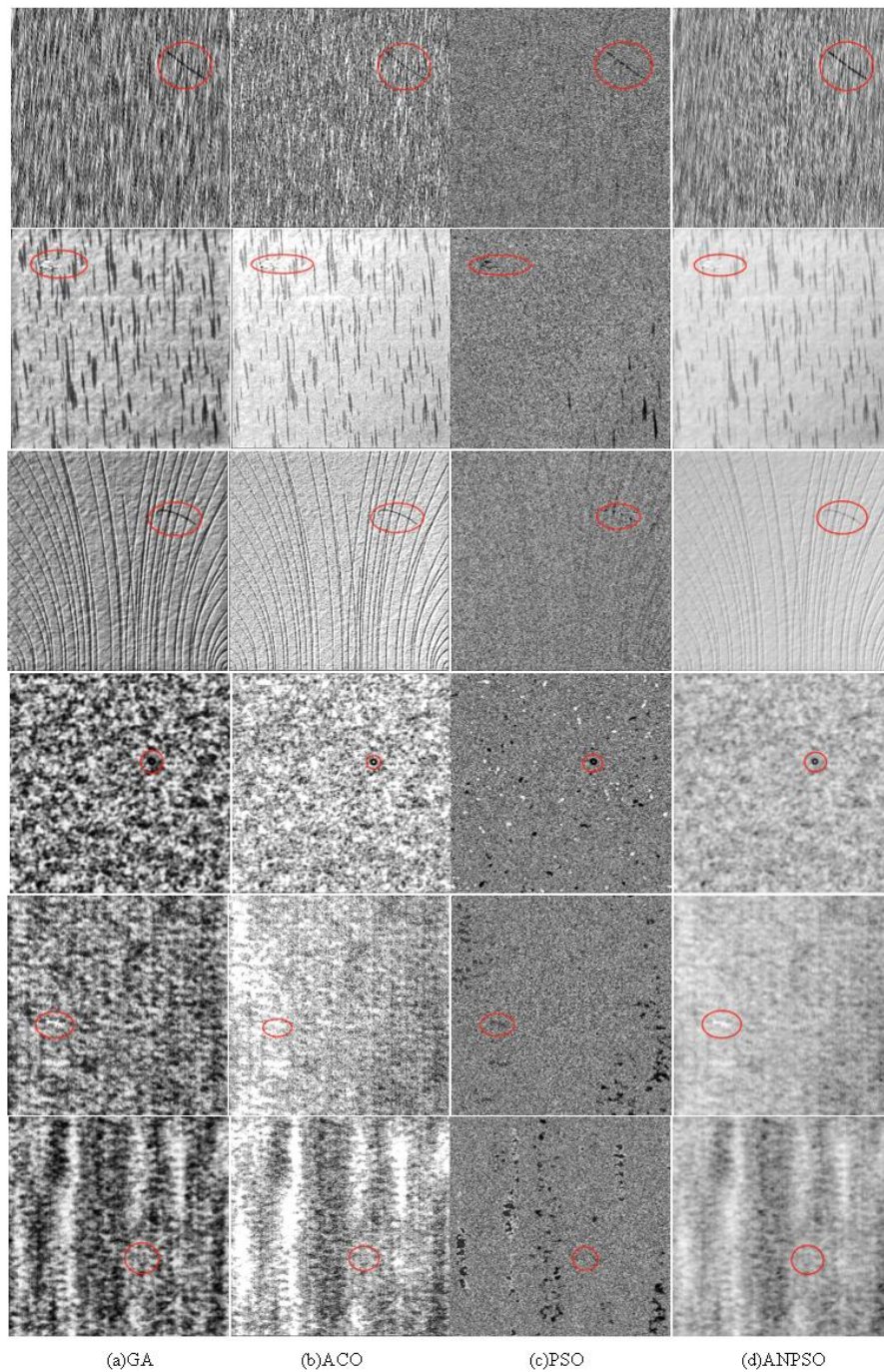
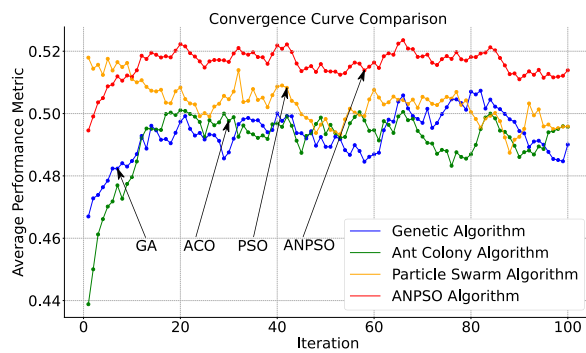
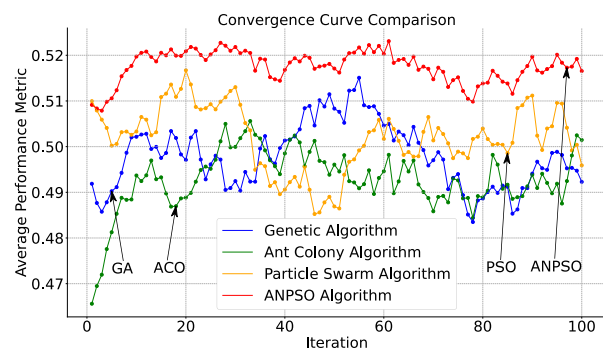


Fig. 9 Comparison of Surface Defect Image Enhancement Effects for Four Types of Products



(a) Convergence Curve of Test Image 1



(b) Convergence Curve of Test Image 2



Fig. 10 Comparison of Convergence Performance of Four Algorithms using LGE Transformation

C. Convergence and Stability Comparison of Algorithms

Fig. 10 below shows the comparison of four optimization algorithms in terms of convergence performance. A higher convergence index reached within a certain number of iterations indicates better convergence performance of the algorithm. As shown in the Fig.10, in the 6 comparison experiments on the convergence of optimization algorithms, the ANPSO proposed in this paper outperformed the traditional 3 image enhancement optimization algorithms (i.e., GA, ACO, and PSO algorithms) in terms of convergence performance, with an average improvement of about 9.7% over the other 3 traditional algorithms in the 100-iteration test. The curves in the figure also indicate that in the 6 comparison experiments, the stability of the ANPSO algorithm is significantly better than the other 3 algorithms.

V. Summary

To improve the efficiency and effectiveness of image enhancement, a novel Ant Colony Natural Inspired Particle Swarm Optimization (ANPSO) algorithm has been proposed, leading to the following conclusions: 1) By integrating Ant Colony Optimization (ACO) and Particle Swarm Optimization (PSO) through natural inspiration and chaos theory, the image enhancement effect can be significantly improved; 2) An adaptive inertia weight adjustment based on a nonlinear random incremental method has been designed, enhancing global search capability and stability; 3) The PSO information transmission mechanism has been improved based on the pheromone release and path optimization mechanisms of the ant colony algorithm, which enhances the efficient sharing of information among particles and strengthens cooperative search abilities. Experimental results show that, compared to Genetic Algorithm (GA), ACO, and PSO, ANPSO has significantly improved key performance indicators, with PSNR, SSIM, and algorithm convergence increasing by 8.3%, 7.6%, and

9.7%, respectively.

References

- [1] W. Zhang, N. Qi, J. Ma, & A. Xiao. "Neural integrated control for a free-floating space robot with suddenly changing parameters". Science China Information Sciences, vol.54, pp.2091-2099, 2011.
- [2] X. Guo, W. Zhang and F. Gao. "Global Prescribed-Time Stabilization of Input-Quantized Nonlinear Systems via State-Scale Transformation". Electronics, vol.12, no.15, pp.3357, 2023.
- [3] W. Zhang, X. Ye, & X. Ji. "RBF neural network adaptive control for space robots without speed feedback signal". Transactions of the Japan Society for Aeronautical and Space Sciences, vol.56, no.6, pp.317-322, 2013.
- [4] Y. Fang, W. Zhang and X. Ye, "Variable structure control for space robots based on neural networks". International Journal of Advanced Robotic Systems, vol.11, no.3, pp.35, 2014.
- [5] W. Zhang, Z. Wen, Y. Ye and S. Zhou, Structural mechanics analysis of bolt joint of rigid flexible coupling manipulator. Journal of Measurements in Engineering, vol.10, no.2, pp.93-104, 2022.
- [6] N. Qi, W. Zhang, J. Gao, & J. Ma. "Design of ground simulation test system for three-dimensional spatial microgravity environment". Jixie Gongcheng Xuebao(Chinese Journal of Mechanical Engineering), vol.47, no.9, pp.16-20, 2011.
- [7] W. Zhang, Z. Wen, Y. Ye, J. Shen, & Ye, X. "Dynamic and vibration characteristics of flexible robot manipulator under complex electromechanical coupling". Journal of Measurements in Engineering, vol.10, no.4, pp.199-214, 2022.
- [8] T. Arici, S. Dikbas and Y. Altunbasak. "A histogram modification framework and its application for image contrast enhancement". IEEE Transactions on image processing, vol.18, no.9, pp.1921-1935, 2009.
- [9] S. Hashemi, S. Kiani, N. Noroozi and M.E. Moghaddam. "An image contrast enhancement method based on genetic algorithm". Pattern Recognition Letters, vol.31, no.13, pp.1816-1824, 2010.
- [10] S. Sahu, A.K. Singh, S.P. Ghrera and M. Elhoseny. "An approach for de-noising and contrast enhancement of retinal fundus image using CLAHE". Optics & Laser Technology, vol.110, pp.87-98, 2019.
- [11] W. Wang, Z. Chen, X. Yuan and X. Wu. "Adaptive image enhancement method for correcting low-illumination images". Information Sciences, vol.496, pp.25-41, 2019.
- [12] J. Shen, W. Zhang, S. Zhou and X. Ye, "Fuzzy adaptive compensation control for space manipulator with joint flexibility and dead zone based on neural network". International Journal of Aeronautical and Space Sciences, vol.24, no.3, pp.876-889, 2023.
- [13] J. Shen, W. Zhang, S. Zhou and X. Ye, "Fuzzy adaptive compensation control for space manipulator with joint flexibility and dead zone based on neural network". International Journal of Aeronautical and Space Sciences, vol.24, no.3, pp.876-889, 2023.

- [14] Y. Hu and W. Zhang, "Modeling framework for analyzing midair encounters in hybrid airspace where manned and unmanned aircraft coexist". Proceedings of the Institution of Mechanical Engineers, Part G: Journal of Aerospace Engineering, vol.233, no.15, pp.5492-5506, 2019.
- [15] C. Narmatha, S.M. Eljack, A.A.R.M. Tuka, S. Manimurugan and M. Mustafa, 2020. "A hybrid fuzzy brain-storm optimization algorithm for the classification of brain tumor MRI images". Journal of ambient intelligence and humanized computing, pp.1-9, 2020.
- [16] P. Zhuang, C. Li and J. Wu. "Bayesian retinex underwater image enhancement". Engineering Applications of Artificial Intelligence, vol.101, pp.104171, 2021.
- [17] F. Orujov, R. Maskeliūnas, R. Damaševičius and W.J.A.S.C. Wei. "Fuzzy based image edge detection algorithm for blood vessel detection in retinal images". Applied Soft Computing, vol.94, pp.106452, 2020.
- [18] D. Wang, D. Tan and L. Liu. "Particle swarm optimization algorithm: an overview". Soft computing, vol.22, pp.387-408, 2018.
- [19] Y. Feng, G.F. Teng, A.X. Wang, and Y.M. Yao. "Chaotic inertia weight in particle swarm optimization". In Second International Conference on Innovative Computing, Information and Control (ICICIC 2007), pp.475-475, IEEE, 2007.
- [20] M. Dorigo, M. Birattari, and T. Stutzle. "Ant colony optimization". IEEE computational intelligence magazine, vol.1, no.4, pp.28-39, 2006.
- [21] D.R.I.M. Setiadi. "PSNR vs SSIM: imperceptibility quality assessment for image steganography". Multimedia Tools and Applications, vol.80, no.6, pp.8423-8444, 2021.

**Zhangping You** works as a professor in the School of School of Engineering at Lishui University. He received a bachelor's degree in Mechanical Design, Manufacturing, and Automation from Changsha University of Science and Technology in 2001, a master's degree in in Mechanical Design and Theory in 2004, and a PhD in Mechatronic Engineering from Tongji University in 2011. His research interests include intelligent control of mechatronic systems, equipment condition monitoring, and fault diagnosis, etc.

**Dajian Yi** is currently a master's student in the School of Mechanical Engineering at Zhejiang Sci-Tech University. He received his bachelor's degree from Lishui University in 2022. Her research focuses on machine vision and mechatronics integration.

**Fang Zheng** works as a senior engineer at Lishui Power Supply Company. He received a bachelor's degree in Industrial Automation from Wuhan University of Water Resources and Electric Power in 2001. His research interests include mechatronics design, computer technology and applications, etc.

**Wenhui Zhang** works as a professor in the School of Electronic Engineering at Nanjing Xiaozhuang University. He received a bachelor's degree in Mechanical Design, Manufacturing, and Automation from Harbin Institute of Technology in 2004, a master's degree in Aerospace Engineering in 2008, and a PhD in Aerospace Science and Technology in 2011. His research interests include robotics technology and intelligent control, machine vision and mechatronics integration technology, etc.